6

Infrared Spectroscopic Ellipsometry for Ion-Implanted Silicon Wafers

Bincheng Li[1] and Xianming Liu[1, 2]
[1]*Institute of Optics and Electronics, Chinese Academy of Sciences, Chengdu*
[2]*The Key Laboratory for Optoelectronic Technologies and Systems of Ministry of Education, Chongqing University, Chongqing China*

1. Introduction

Spectroscopic ellipsometry (SE) is an optical technique that measures changes in the reflectance and phase differences between the parallel (*Rp*) and perpendicular (*Rs*) components of a polarized light beam upon reflection from a surface. As a non-contact and non-destructive optical method, SE is widely used to determine the thickness and optical constants (refractive index *n* and extinction coefficient *k*) of films or layered structures, as well as other properties related to optical constants.

Spectroscopic ellipsometry was firstly applied to analyze the optical properties of implanted silicon wafer back in 1979. From then on the SE technique has been widely used in characterization of mono-, micro-, and poly- crystalline, and amorphous silicon wafers, and in implantation and annealing process monitoring. Up to now, most researches were focused on the visible spectral range as implantation induced lattice damage altered the optical properties of implanted silicon wafers in the visible range. However, when the implanted silicon wafers were thermally annealed, their optical properties in the visible range were restored to that of monocrystalline silicon. Visible SE can no longer distinguish between silicon wafers implanted with different dose or energy. On the other hand, Infrared spectroscopic ellipsometry (IRSE) could be a sensitive characterization technique for implanted silicon wafers, as in the infrared spectral range, the optical properties of the implanted silicon wafers are functions of the activated impurity concentration, which is a function of the implantation dose or energy.

In this chapter, the principle of ellipsometry is introduced briefly in section 2. The application of visible spectroscopic ellipsometry to characterize silicon wafers is reviewed in section 3. In section 4, IRSE spectra of implanted silicon wafers with and without thermal annealing are analyzed comparatively. An equivalent optical model is established to fit the IRSE spectra for implanted and annealed silicon wafers. Finally, a summary is presented in section 5.

2. Principle of ellipsometry

Spectroscopic ellipsometry is a sensitive optical technique for determining optical and structural properties of layered surfaces and thin films. In this section, a brief introduction to the principle of ellipsometry measurement is presented.

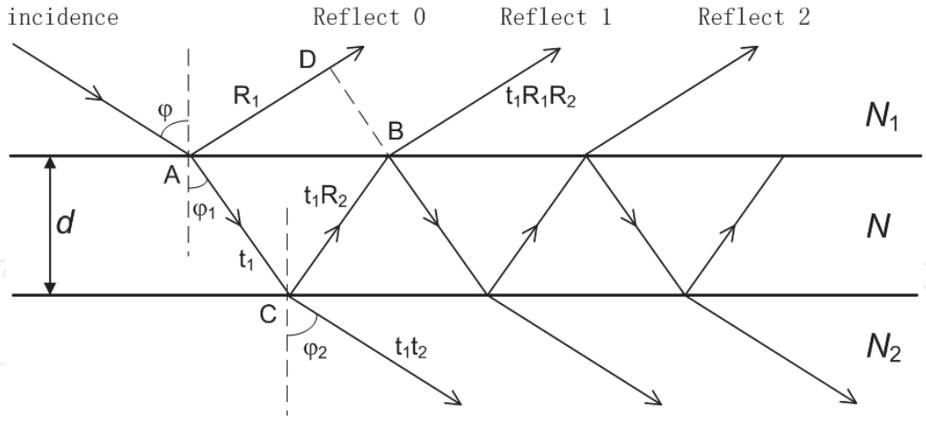

Fig. 1. Reflection and transmission of a transparent plate

When linearly polarized light of a known orientation is reflected or transmitted at oblique incidence from an interface, the reflected or transmitted light becomes elliptically polarized. The orientation and shape of the ellipse depend on the direction of the polarization of the incident light, the angle of incidence, and the optical properties of the interface. Based on the electric field components polarized parallelly (*p*) or perpendicularly (*s*) to the plane of incidence, the polarized light can be classified as *p*- and *s*- polarized light.

Taking a transparent plate for example, the incident light was divided into reflected light and refracted light at the surface of a sample when a monochromatic beam with wavelength λ was incident as show in Fig. 1. Every encounter with the interface of the beam would have a decomposition, therefore, the total reflected light is the summation of the multiple reflection and refraction of light 0, 1, 2, ... , n.

Here, assume d is the plate thickness and $N=n+ik$ is the complex refractive index of the plate, with n the refractive index and k the extinction coefficient. The complex refractive indexes of the medium on both sides of the plate are N_1 and N_2, respectively. The optical path difference l_0 between the reflected beam 0 and the reflected beam 1 is:

$$l_0 = N \cdot (\overline{AC} + \overline{AB}) - N_1 \cdot \overline{AD} \tag{1}$$

where

$$\overline{AC} = \overline{CB} = \frac{d}{\cos\varphi_1} \tag{2}$$

$$\overline{AD} = 2d \tan\varphi_1 \sin\varphi_1 = \frac{2dn\sin^2\varphi_1}{\cos\varphi_1} \tag{3}$$

and

$$l_0 = 2dN\cos\varphi_1 \tag{4}$$

The corresponding phase difference is

$$\delta = \frac{2\pi l_0}{\lambda} = \frac{4\pi d}{\lambda} \cdot \sqrt{N^2 - \sin^2\varphi_1} \tag{5}$$

According to Fresnel reflection formula, the reflective index of *p*-component and *s*-component at two surfaces of the sample can be deduced as follows:

$$r_{1p} = \frac{N\cos\varphi - N_1\cos\varphi_1}{N\cos\varphi + N_1\cos\varphi_1} \tag{6}$$

$$r_{1s} = \frac{N_1\cos\varphi - N\cos\varphi_1}{N_1\cos\varphi + N\cos\varphi_1} \tag{7}$$

$$r_{2p} = \frac{N_2\cos\varphi_1 - N\cos\varphi_2}{N_2\cos\varphi_1 + N\cos\varphi_2} \tag{8}$$

$$r_{2s} = \frac{N\cos\varphi_1 - N_2\cos\varphi_2}{N\cos\varphi_1 + N_2\cos\varphi_2} \tag{9}$$

Assume that the amplitudes of *p*- and *s*-components of the incident beam and the reflected beam are E_{ip} , E_{is} , E_{rp} , E_{rs}, respectively, while

$$R_p = \frac{E_{rp}}{E_{ip}};\ \ R_s = \frac{E_{rs}}{E_{is}} \tag{10}$$

The ratio of the total reflectance of *p*-component and *s*-component is:

$$\frac{R_p}{R_s} = \frac{E_{rp}/E_{ip}}{E_{rs}/E_{is}} = \frac{(E_p/E_s)_r}{(E_p/E_s)_i} e^{i(\beta_r - \beta_i)} \tag{11}$$

Where $\beta_i = (\beta_p - \beta_s)_i$ is the phase difference of *p*- and *s*-components in the incident light, and $\beta_r = (\beta_p - \beta_s)_r$ is the phase difference of *p*- and *s*-components in the reflected light. Define

$$\tan\Psi = \frac{(E_p/E_s)_r}{(E_p/E_s)_i} \tag{12}$$

$$\Delta = \beta_r - \beta_i \tag{13}$$

then

$$\frac{R_p}{R_s} = \tan\Psi \cdot e^{i\Delta} \tag{14}$$

where tanΨ means the attenuation of the relative amplitudes of *p*- and *s*-components after being reflected on each surface (or interface) while Δ means the phase difference change through this process, both of which can be measured by an ellipsometer directly.

Taking multiple reflection and refraction on the surface of the sample into account and combining Fresnel formula, the total reflection coefficients of *p*- and *s*-components are

$$R_p = \frac{r_{1p} + r_{2p}\exp(-i\delta)}{1 + r_{1p}r_{2p}\exp(-i\delta)} \tag{15}$$

$$R_s = \frac{r_{1s} + r_{2s}\exp(-i\delta)}{1 + r_{1s}r_{2s}\exp(-i\delta)} \tag{16}$$

Ellipsometric equation can be represented by

$$\begin{aligned} \tan\Psi \cdot e^{i\Delta} &= \frac{R_p}{R_s} = \frac{r_{1p} + r_{2p}\exp(-i\delta)}{1 + r_{1p}r_{2p}\exp(-i\delta)} \cdot \frac{1 + r_{1s}r_{2s}\exp(-i\delta)}{r_{1s} + r_{2s}\exp(-i\delta)} \\ &= f(N_1, N_2, N, \varphi, d, \lambda) \end{aligned} \tag{17}$$

which shows the relationship between the variation of polarization state Ψ, Δ and the thickness d, the complex refractive index N. Here both Ψ and Δ are called ellipsometric parameters, each of which has an angular value. Since N_1, N_2, λ and φ are known parameters, and Ψ and Δ can be measured experimentally, N and d can be determined by a least-square fitting calculation. This is the foundation of calculating the sample's thickness and complex refractive index by the ellipsometric data.

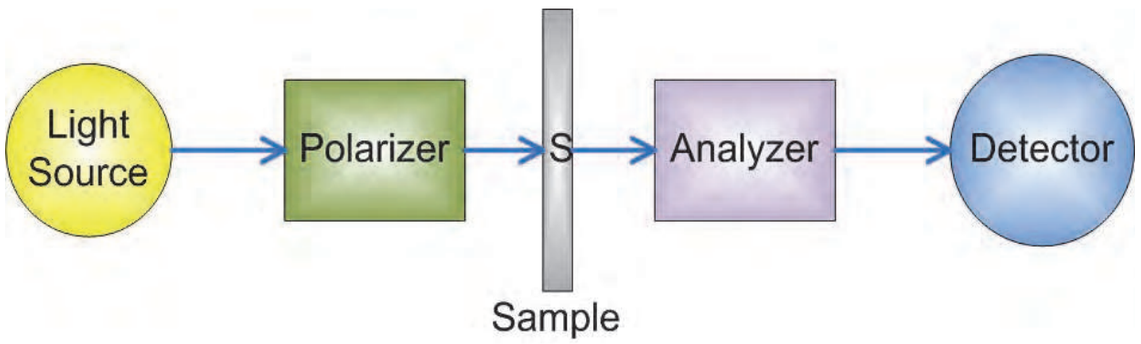

Fig. 2. Schematic diagram of a general spectroscopic ellipsometric arrangement

The changes of the polarization direction of the reflected or transmitted light can be measured with a spectroscopic ellipsometer, by which the relative amplitude and phase change introduced by the interface can be calculated. The schematic diagram of a general spectroscopic ellipsometric arrangement is shown in Fig. 2.

A collimated monochromatic or quasi-monochromatic beam from a light source passes through a variable angle polarizes to produce light of known controlled polarization. The light interacts with the sample under study and its polarization is modified. The modified state of polarization at the output of the system is analyzed by a variable polarization analyzer and can be measured by a photo-detector. Then, an equal optical model that can accurately represent the true physical structure of the sample under study should be developed to interpret the measured data. Finally, the optical and structural parameters of the sample can be obtained by solving an inverse problem.

As spectroscopic ellipsometry is a powerful and versatile non-contact and non-destructive technique for the investigation of the optical properties and structural parameters of thin films or layered structures, it has found wide applications in many different fields, from semiconductor physics to microelectronics and biology, from basic research to industrial applications, etc.. In the following sections, some typical applications of spectroscopic ellipsometry on the measurements of semiconductor silicon are presented.

3. Visible and near infrared ellipsometry

Spectroscopic ellipsometry is sensitive to the optical properties of the film deposited on a substrate. Therefore the physical or chemical properties which link to the optical properties of the sample can be characterized by spectroscopic ellipsometry.

In integrated circuits (IC) manufacturing, silicon wafers were doped by ion implantation to improve their electrical properties. Implantation induced damage altered the optical properties of the silicon wafers in the visible spectral range. Therefore, most spectroscopic ellipsometry measurements on implanted silicon wafers were carried out in the visible spectral range. In the past few decades, spectroscopic ellipsometry was applied to characterize the damage depth profiles, the surface and interface, and the structural changes of the silicon wafers.

As the SE measured damage is introduced by ion implantation, implantation parameters, such as the implantation dose and energy, can therefore be obtained indirectly. In visible spectral range, spectroscopic ellipsometry has been widely used for *in-situ* monitoring of ion implantation dose. As early as the 1980s, spectroscopic ellipsometry was applied to investigate the As^+ and P^+ ion implanted silicon wafers at wavelengths in the range of 325-400 nm. Results have shown that the ellipsometric spectra in this spectral range were very sensitive to the lattice damages introduced by ion implantation. Both implantation dose and energy could be determined by visible SE. In several research papers the monitoring of implantation energy by visible spectroscopic ellipsometry were reported. Spectroscopic ellipsometry could also be used in thin film deposition processes, such as the growth of microcrystalline silicon. The measurements were carried out in the 2.5-5eV (248-496nm) spectral range.

In our work, five groups (G1 to G5) of silicon wafers with properties shown in Table 1 were prepared under different process conditions. All substrates were prepared from the same batch of <111> oriented p-type Czochralski crystalline silicon wafers, (525±20μm, 8-13Ω·cm), with the front surface chemically-mechanically polished. These samples were implanted with As+ ions. G1 and G2 were implanted with implantation doses from 1×10^{11} to $1\times10^{16}/cm^2$ at the same implantation energy of 100keV. G3 and G4 were implanted with implantation energies from 20 to 140keV at implantation dose of $1\times10^{15}/cm^2$. All wafers of G5 were implanted with $1\times10^{15}/cm^2$ at 100keV. After implantation, G1 and G3 were then annealed in a rapid thermal annealing (RTA) system for 30s at 1100℃ in an inert nitrogen atmosphere, and G2 and G4 were not annealed. Wafers in G5 were annealed at various temperatures ranging from 500 to 1100℃ for 30s.

Wafer group	Implantation dose (As^+/cm^2)	Implantation energy (keV)	Annealing temperature (℃)
G1	1×10^{11} - 1×10^{16}	100	--
G2	1×10^{11} - 1×10^{16}	100	1100
G3	1×10^{15}	20 - 140	--
G4	1×10^{15}	20 - 140	1100
G5	1×10^{15}	100	500 - 1100

Table 1. List of wafer groups prepared with different implantation and annealing conditions

The SE measurements were performed with a generalized ellipsometer at room temperature. The spectral range from 270 to 2000 nm was covered using a rotating-analyzer ellipsometer with automated compensator function (VASE®, J. A. Woollam). All measurements were carried out at an angle of incidence of 75°.

The ellipsometric spectra of ion implanted wafers with different implantation doses without annealing were plot in Fig. 3. The optical properties in the visible spectral range were altered by ion implantation for wafers with implantation dose higher than $10^{14}cm^{-2}$. However, when these highly implanted wafers were annealed at high temperature, the visible ellipsometry (300-800nm) could no longer distinguish the wafers with different implantation doses, even for wafers implanted with a high dose. The visible ellipsometric spectra of ion implanted wafers were close to that of monocrystalline silicon, as presented in Fig. 4.

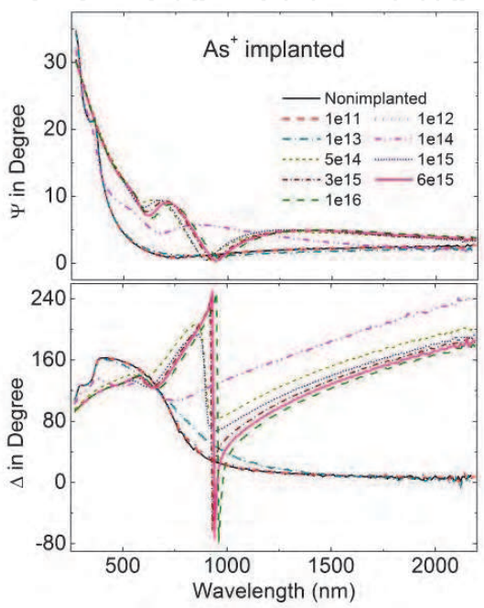

Fig. 3. Ellipsometric spectra of wafers G1 in visible and near infrared range at 75°.

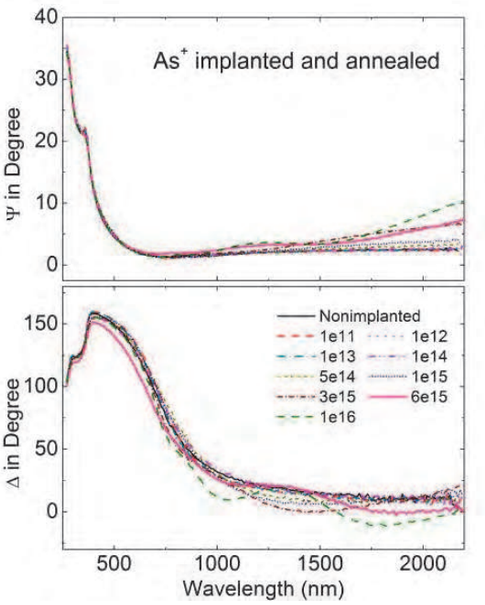

Fig. 4. Ellipsometric spectra of wafers G2 in visible and near infrared range at 75°.

Figure 5 presented the ellipsometric spectra for wafers implanted with different implantation energies. The implanted layer influenced the visible ellipsometric spectra, and

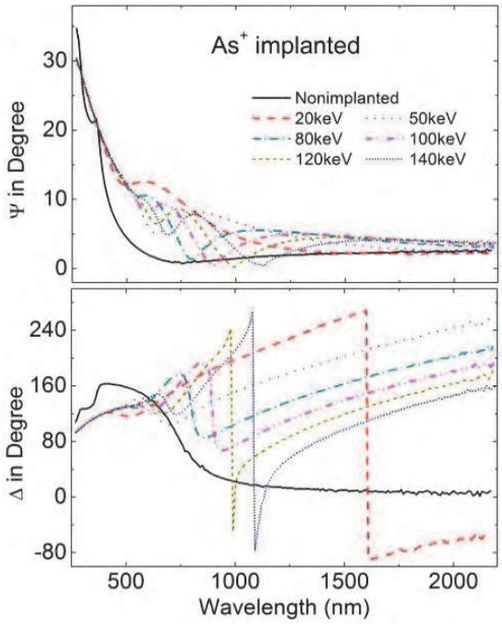

Fig. 5. Ellipsometric spectra of wafers G3 in visible and near infrared range at 75°.

the layer thickness was determined by implantation energy. Similar to that in Fig. 4, the visible ellipsometric spectra for annealed wafers with different implantation energies were close to that of non-implanted monocrystalline silicon, as shown in Fig. 6. Ellipsometric spectra for wafers annealed at different temperature were plot in Fig. 7. Spectra of wafers

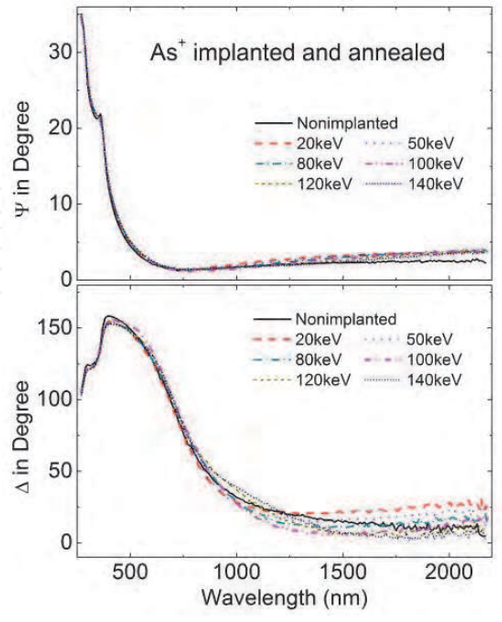

Fig. 6. Ellipsometric spectra of wafers G4 in visible and near infrared range at 75°.

prepared with the same implantation conditions but without thermal annealing were shown for comparison. When the implanted wafers were thermally annealed, the temperature of 600℃ was considered to be a threshold, above this annealing temperature the damaged material was reconstructed and returned to its original crystal structure. Thus the annealing temperature of 1100℃ in our process made the implantation induced structural damage almost totally recrystallized.

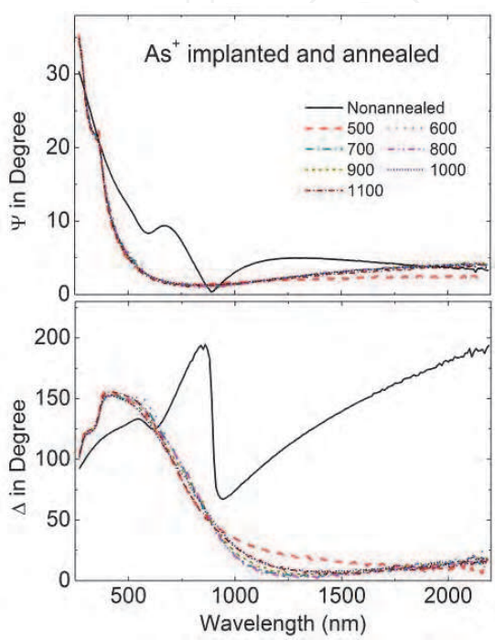

Fig. 7. Ellipsometric spectra of wafers G5 in visible and near infrared range at 75°. For comparison, the spectra of a non-annealed reference wafer were shown by the solid lines.

4. Infrared spectroscopic ellipsometry

The results reported in section 3 indicated that the visible SE is not a sensitive method to investigate the ion implantation induced effects of ion-implanted silicon wafers which were completely annealed. In practice, however, during the ICs processing, ion implantation is the predominant doping method to alter the electrical properties. It is always followed by thermal annealing to recrystallize the damaged material and active the impurities. Evaluating the distribution of the implanted ions and the activated impurities after ion implantation and thermal annealing is essential for the semiconductor device design, simulation and fabrication. From section 3 it is noticed that the effects of implantation dose and energy on the SE parameters begin to be evident from the near infrared range, as shown in Fig. 4. It is of interest to extend the SE measurement into the infrared spectral range.

The infrared spectroscopic ellipsometry measurements were carried out in the 300-5000cm^{-1} (2-30μm) spectral range by a rotating-polarizer, rotating-compensator, Fourier-transform based variable angle spectroscopic ellipsometer (IR-VASE®, J. A. Woollam Co.) at room temperature. The angle of incidence was set to 75° to keep in consistence with the SE measurements performed in the visible spectral range. The same wafers used in Section 3

were comparatively studied in the infrared spectral range, with the ellipsometric spectra of wafers G1-G5 were presented in Fig. 8 to Fig. 12.

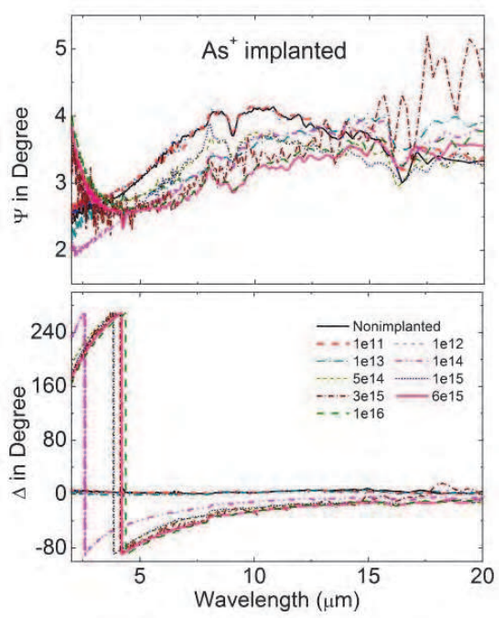

Fig. 8. Ellipsometric spectra of wafers G1 in the infrared range at 75°.

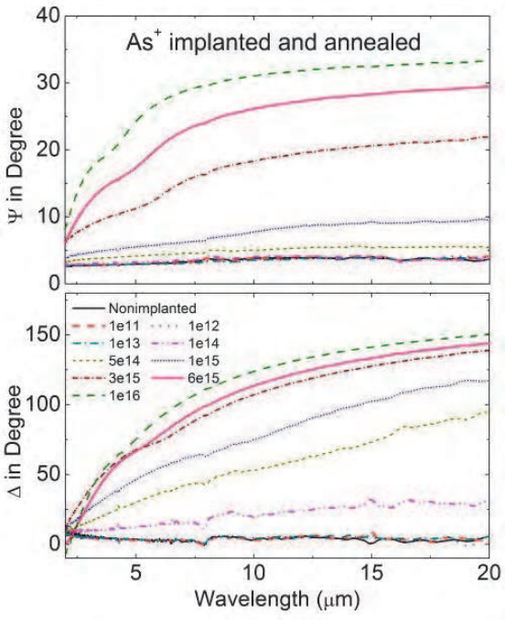

Fig. 9. Ellipsometric spectra of wafers G2 in the infrared range at 75°.

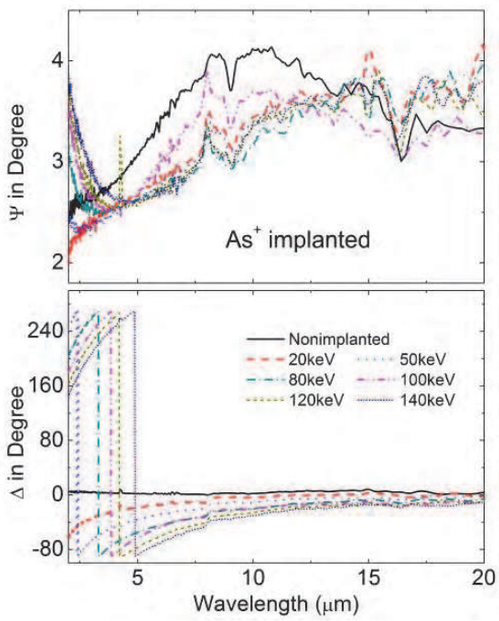

Fig. 10. Ellipsometric spectra of wafers G3 in the infrared range at 75°.

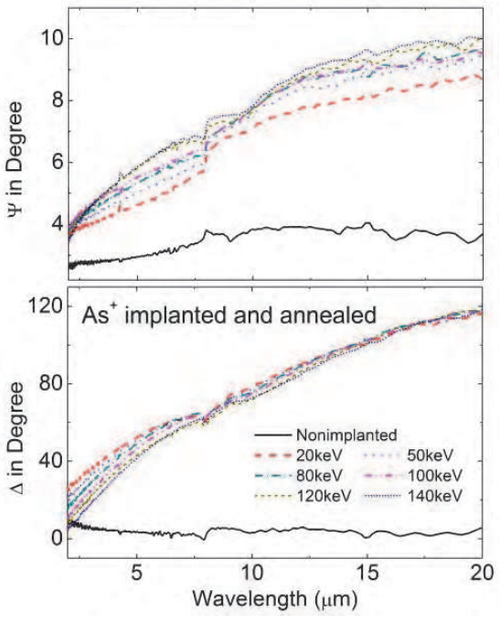

Fig. 11. Ellipsometric spectra of wafers G4 in the infrared range at 75°.

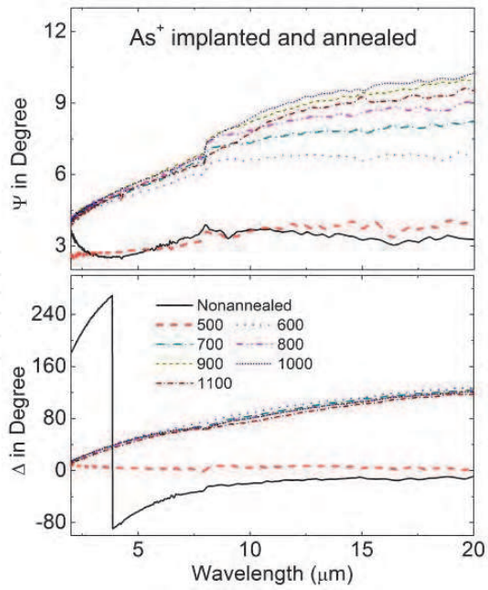

Fig. 12. Ellipsometric spectra of wafers G5 in the infrared range at 75°. For comparison, the spectra of a non-annealed reference wafer were shown by the solid lines.

In opposition to the results obtained in the visible spectral range, as presented in section 3, the IRSE is not a sensitive method for implanted wafers without thermal annealing. The value of ellipsometric parameter Ψ ranged only 2-4°, as shown in Fig. 8, Fig. 10, and Fig. 12. The results indicated that ion implantation alone introduced no significant change to the optical properties of damaged crystal structure in the infrared range. However, once the implanted wafers were thermally annealed at high temperature, the IRSE could effectively distinguish the wafers with different implantation doses, especially for wafers implanted with a high dose, as presented in Fig. 9. On the other hand, the IRSE could not clearly distinguish the wafers implanted with different energies, as shown in Fig. 11. In the following, the infrared ellipsometric spectra for implanted and annealed wafers were analyzed in details.

In the infrared range, different absorption processes exist in a silicon wafer, such as free carrier absorption, impurity absorption and Reststrahlen absorption, as shown in Fig. 13.

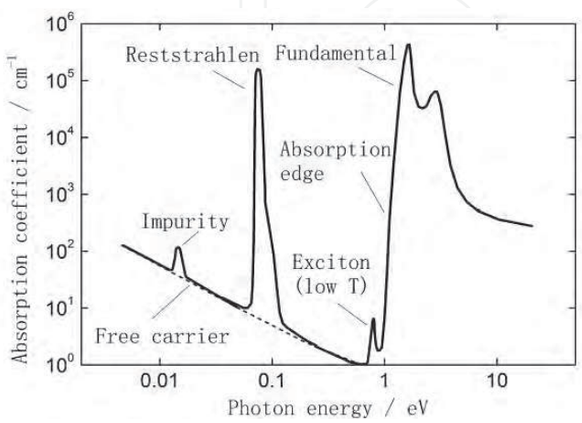

Fig. 13. Absorption coefficient plotted as a function of the photon energy in a silicon wafer, illustrating various possible absorption processes

At room temperature for silicon, the impurity absorption is too weak to be observed. The influence of the Reststrahlen absorption process on the optical properties of implanted silicon wafer is at least two orders of magnitude lower than the influence of the free carrier absorption, thus is negligible. Therefore, the free carrier absorption dominates the optical properties of the implanted layer in the infrared range, which can be described by a classical Drude model:

$$\tilde{\varepsilon}\left(E=\hbar\omega\right)=\frac{-\hbar^2}{\varepsilon_0\rho\left(\tau\cdot E^2+i\hbar E\right)} \tag{18}$$

with

$$\begin{aligned}\rho&=\frac{1}{eN\mu},\\ \mu&=e\tau/m^*,\\ m&=m^*/m_0\end{aligned} \tag{19}$$

where ε is the complex dielectric constant, ε_0 is the vacuum dielectric constant, N is the carrier concentration, e is the electronic charge, m^* is the ratio of the optical carrier effective mass to the electron rest mass, E is the energy of the incident photons, ρ is the resistivity, and τ is the mean scattering time of the free carriers. The parameters Ψ and Δ can be implicitly expressed as a function of the dielectric function ε and the thickness of the wafer under study.

In order to simulate the optical properties of the ion implanted silicon wafer, the atoms distribution was calculated. The calculation was performed with the Monte Carlo simulation by software package TRIM. Figure 14 shows the simulation results as well as the corresponding Gaussian fit for an As^+ implanted silicon wafer.

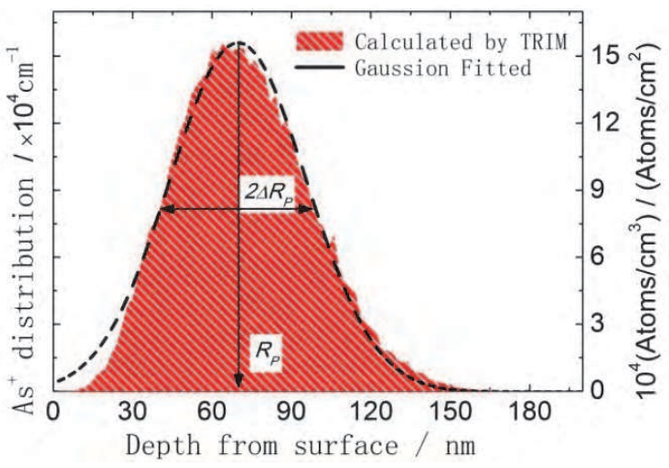

Fig. 14. Calculated As^+ ion distribution and corresponding Gaussian fitted result.

The As^+ ion distribution can be expressed with a Gaussian function:

$$N=N_{\max}\exp[-\frac{1}{2}(\frac{d-R_p}{\Delta R_p})^2], \tag{20}$$

where N_{max} is the maximum carrier concentration, d is the depth, R_p is the range, and ΔR_p is the standard deviation of the Gaussian function. The Gaussian fitted curve is plot in Fig. 14. The fitted values are given in Table 2.

Fitted parameter	Fitted value	Fitting error
R_p (nm)	69.78909	0.2599
ΔR_p (nm)	25.8049	0.32895
A（corresponding N_{max}）	15.63882	0.15216

Table 2. As^+ ion distribution parameters fitted with a Gaussian function.

For the evaluation of IRSE data of these implanted wafers, the optical model with an ion-implanted layer described by 30 sub-layers, and a single-crystalline silicon substrate layer is employed to describe the structure of the implanted wafer. Although both the m^* and τ are functions of the doping concentration, it is reasonable to consider them as fixed values in the ion-implanted layer in each fitting. The optical properties of the ion implanted layer can be expressed by the Drude model, while the optical properties of the substrate silicon in the infrared range can be taken from literature (Palik, 1998). Then, the ion distribution parameters and the physical properties of the implanted layer can be fitted. In the multi-parameter fitting program, a mean square error (MSE) was minimized. The MSE was defined as:

$$MSE^2 = \frac{1}{2n-p}\sum_{i=1}^{n}\left[\left(\tan\Psi_i^{\mathrm{mod}} - \tan\Psi_i^{\mathrm{exp}}\right)^2 + \left(\cos\Delta_i^{\mathrm{mod}} - \cos\Delta_i^{\mathrm{exp}}\right)^2\right] \tag{21}$$

Here, *mod* and *exp* represent the data calculated from the theoretical model and the experimental data, respectively. n is the number of measured ψ and Δ pairs being included in the fitting and p is the number of fitting parameters. In this multi-parameter fitting, six parameters are set as free parameters to minimize the MSE, that is, N_{max}, R_p, ΔR_p, m, μ and the implanted layer thickness l.

To reduce the number of iteration and improve the computation efficiency in the multi-parameter fitting procedure, it is important to give a reasonable initial set of values for the free parameters in the fitting. Here, R_p and ΔR_p values fitted in Table 2 are set as the initial values. For N_{max}, the initial value is $\frac{dose}{\sqrt{2\pi}\cdot\Delta R_p}$. As shown in Fig. 9, only the annealed wafers in G2 with As^+ ion implantation dose higher than 1×10^{14} cm^{-2} can be distinguished by infrared ellipsometric spectra, which are fitted with above model. The optimized fitted parameters for the ion-implanted layers of wafers implanted with different doses are listed in Table 3, in which the ρ and τ values are calculated with the fitted values. The IRSE fitted results for wafers in Table 3 are shown in Fig. 15 by the solid lines. The units of the horizontal abscissa are wave number, in accordance with the measurement conditions of the infrared ellipsometer. Good agreements between the experimental SE data and the best fits are observed in this spectral range.

From Table 3, it is observed that the impurities were activated by the rapid thermal annealing, which resulted in the redistribution. For implanted wafers with higher doses, more impurities were activated and the impurities diffused farther. Therefore, the N_{max}, R_p and ΔR_p of the implanted layer increased with the increasing implantation dose, especially for wafers with high implantation doses. Meanwhile, the mean scattering time of the free carriers decreased due to the increasing impurity concentration.

Dose (cm^{-2})	1×10^{14}	5×10^{14}	1×10^{15}	3×10^{15}	6×10^{15}	1×10^{16}
l (nm)	118.1	152.2	166.5	171.9	249.6	252.2
R_p (nm)	60.4	66.1	62.3	62.9	85.9	97.5
ΔR_p (nm)	65.6	64.8	66.1	73.6	99.2	104.8
N_{max} (cm^{-3})	8.3×10^{18}	2.8×10^{19}	9.9×10^{19}	3.2×10^{20}	7.3×10^{20}	1.5×10^{21}
μ ($cm^2/V\cdot s$)	166.6	58.4	26.6	20.1	11	7.2
m	0.36	0.37	0.67	0.78	1.43	1.95
ρ ($10^{-3}\Omega\cdot cm$)	4.51	3.82	2.37	0.97	0.78	0.58
τ (fs)	34.06	12.15	10.1	8.96	8.95	7.99
MSE	0.386	0.316	0.257	0.21	0.302	0.276

Table 3. Best-fit model parameters of the ion-implanted layer. ρ and τ are calculated with the fitted values.

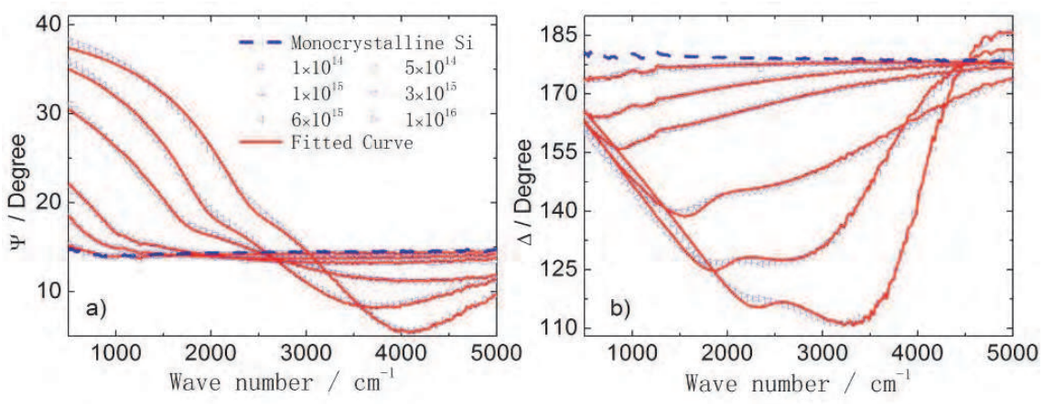

Fig. 15. The measured and best-fitted infrared ellipsometric spectra Ψ and Δ for silicon wafers As^+ implanted with different doses.

5. Conclusion

In this chapter the application of spectroscopic ellipsometry to silicon characterization and processes monitoring has been reviewed. The comparative studies on the infrared spectroscopic ellipsometry for implanted silicon wafers with and without thermal annealing have been presented. Several conclusions can be summarized as follows:

- For implanted but non-annealed silicon wafers, the optical properties in the visible spectral range are determined by ion implantation induced lattice damages.
- For implanted and annealed silicon wafers, the optical properties in the visible spectral range are close to that of monocrystalline silicon, as the lattice damages are recovered by thermal annealing.
- In infrared spectral range, the optical properties of the implanted and annealed silicon wafers are functions of the activated impurities concentration, which is determined by the implantation dose, the implantation energy and the annealing temperature.
- The optical properties of the implanted and annealed silicon wafers in the infrared spectral range can be described with a Drude free-carrier absorption equation.

Therefore, the infrared ellipsometric spectra can be analyzed with the corresponding model to better characterize the implanted and annealed silicon wafers.

6. Reference

Palik, E D. (1998). *Handbook of Optical Constants of Solids.* Academic, ISBN 978-012-5444-23-1, San Diego, USA

Watanabe, K; Miyao, M; Takemoto, I & Hashimoto, N. (1979). Ellipsometric study of silicon implanted with boron ions in low doses. *Applied Physics Letters,* Vol. 34, No. 8, pp. 518-519, ISSN 0003-6951

Fried, M; Polgar, O; Lohner, T; Strehlke, S & Levy-Clement, C. (1998). Comparative study of the oxidation of thin porous silicon layers studied by reflectometry, spectroscopic ellipsometry and secondary ion mass spectroscopy. *Journal of Luminescence,* Vol. 80, No. 1-4, pp. 147-152, ISSN 0022-2313

Cabarrocas, P R I; Hamma, S; Hadjadj, A; Bertomeu, J & Andreu, J. (1996). New features of the layer-by-layer deposition of microcrystalline silicon films revealed by spectroscopic ellipsometry and high resolution transmission electron microscopy. *Applied Physics Letters,* Vol. 69, No. 4, pp. 529-531, ISSN 0003-6951

Drevillon, B; Godet, C & Kumar, S. (1987). Insitu Spectroscopic Ellipsometry Investigation of the Nucleation of Microcrystalline Silicon. *Applied Physics Letters,* Vol. 50, No. 23, pp. 1651-1653, ISSN 0003-6951

Kang, T D; Lee, H; Park, S J; Jang, J & Lee, S. (2002). Microcrystalline silicon thin films studied using spectroscopic ellipsometry. *Journal of Applied Physics,* Vol. 92, No. 5, pp. 2467-2474, ISSN 0021-8979

Nelson, F J; Kamineni, V K; Zhang, T; Comfort, E S; Lee, J U & Diebold, A C. (2010). Optical properties of large-area polycrystalline chemical vapor deposited graphene by spectroscopic ellipsometry. *Applied Physics Letters,* Vol. 97, No. 25, pp. 253110-3, ISSN 0003-6951

Fujiwara, H; Koh, J; Wronski, C R & Collins, R W. (1997). Application of real time spectroscopic ellipsometry for high resolution depth profiling of compositionally graded amorphous silicon alloy thin films. *Applied Physics Letters,* Vol. 70, No. 16, pp. 2150-2152, ISSN 0003-6951

Lohner, T; Khanh, N Q; Petrik, P; Fried, M; Kotai, E & Gyulai, J. (1997). Ion implantation induced damage accumulation studied by Rutherford Backscattering Spectrometry and Spectroscopic Ellipsometry. *Materials Science Applications of Ion Beam Techniques,* Vol. 248, No. pp. 229-232, ISSN 0255-5476

Podraza, N J; Li, J; Wronski, C R; Dickey, E C & Collins, R W. (2009). Analysis of controlled mixed-phase, amorphous plus microcrystalline. silicon thin films by real time spectroscopic ellipsometry. *Journal of Vacuum Science & Technology A,* Vol. 27, No. 6, pp. 1255-1259, ISSN 0734-2101

Petrik, P; Polgar, O; Lohner, T; Fried, M; Khanh, N Q & Gyulai, J. (1998). Ion implantation-caused damage depth profiles in single-crystalline silicon studied by Spectroscopic Ellipsometry and Rutherford Backscattering Spectrometry. *Vacuum,* Vol. 50, No. 3-4, pp. 293-297, ISSN 0042-207X

Petrik, P; Lohner, T; Fried, M; Khánh, N Q; Polgár, O & Gyulai, J. (1999). Comparative study of ion implantation caused damage depth profiles in polycrystalline and single crystalline silicon studied by spectroscopic ellipsometry and Rutherford ackscattering spectrometry. *Nuclear Instruments and Methods in Physics Research B,* Vol. 147, No. pp. 84-89, ISSN 0168-583X

Fried, M; Lohner, T; Aarnink, W A M; Hanekamp, L J & van Silfhout, A. (1992). Nondestructive determination of damage depth profiles in ion-implanted semiconductors by spectroscopic ellipsometry using different optical models. *Journal of Applied Physics,* Vol. 71, No. 6, pp. 2835-2843, ISSN 0021-8979

Yamada, T; Harada, N; Kitahara, K & Moritani, A. (2003). Study of mechanism of plasma surface modifications in Si by spectroscopic ellipsometry. *Surface and Coatings Technology,* Vol. 173, No. pp. 854-857, ISSN 0257-8972

McMarr, P J; Vedam, K & Narayan, J. (1986). Spectroscopic ellipsometry: A new tool for nondestructive depth profiling and characterization of interfaces. *Journal of Applied Physics,* Vol. 59, No. 3, pp. 694-701, ISSN 0021-8979

Hikino, S-i & Adachi, S. (2004). Structural changes in ion-implanted and rapid thermally annealed Si(100) wafers studied by spectroscopic ellipsometry. *Journal of Physics D: Applied Physics,* Vol. 37, No. pp. 1617–1623, ISSN 0022-3727

Jans, J C; Hollering, R W J & Lifka, H. (1991). Characterization of Annealed High-Dose Oxygen-Implanted Silicon by Spectroscopic Ellipsometry and Reflectometry. *Journal of Applied Physics,* Vol. 70, No. 11, pp. 6643-6646, ISSN 0021-8979

Petrik, P; Lohner, T; Fried, M; Khanh, N Q; Polgar, O & Gyulai, J. (1999). Comparative study of ion implantation caused damage depth profiles in polycrystalline and single crystalline silicon studied by spectroscopic ellipsometry and Rutherford backscattering spectrometry. *Nuclear Instruments & Methods in Physics Research Section B-Beam Interactions with Materials and Atoms,* Vol. 147, No. 1-4, pp. 84-89, ISSN 0168-583X

Petrik, P; Cayrel, F; Fried, M; Polgar, O; Lohner, I; Vincent, L; Alquier, D & Gyulai, J. (2004). Depth distribution of disorder and cavities in high dose helium implanted silicon characterized by spectroscopic ellipsometry. *Thin Solid Films,* Vol. 455-56, No. pp. 344-348, ISSN 0040-6090

Tsunoda, K; Adachi, S & Takahashi, M. (2002). Spectroscopic ellipsometry study of ion-implanted Si(100) wafers. *Journal of Applied Physics,* Vol. 91, No. 5, pp. 2936-2941, ISSN 0021-8979

Cortot, J P & Ged, P. (1982). Analysis of Arsenic and Phosphorus Ion-Implanted Silicon by Spectroscopic Ellipsometry. *Applied Physics Letters,* Vol. 41, No. 1, pp. 93-95, ISSN 0003-6951

Lioudakis, E; Christofides, C & Othonos, A. (2006). Study of the annealing kinetic effect and implantation energy on phosphorus-implanted silicon wafers using spectroscopic ellipsometry. *Journal of Applied Physics,* Vol. 99, No. 12, pp. 123514-6, ISSN 0021-8979

Hu, Y Z; Li, M; Conrad, K; Andrews, J W; Irene, E A; Denker, M; Ray, M & Mcguire, G. (1992). Insitu Spectroscopic Ellipsometry Studies of Hydrogen-Ion Bombardment of Crystalline Silicon. *Journal of Vacuum Science & Technology B,* Vol. 10, No. 3, pp. 1111-1117, ISSN 1071-1023

Kasap, S & Capper, P. (2006). *Springer Handbook of Electronic and Photonic Materials.* Springer Science, 978-038-7260-59-4, Heidelberg

Tiwald, T E; Thompson, D W & Woollam, J A. (1998). Optical determination of shallow carrier profiles using Fourier transform infrared ellipsometry *Journal of Vacuum Science & Technology B: Microelectronics and Nanometer Structures,* Vol. 16, No. 1, pp. 312-315, ISSN 1071-1023

Ziegler, J F; Biersack, J P & Littmark, U. (1985). *The Stopping Range of Ions in Solids.* Pergamon, ISBN 978-008-0216-03-4, Tarrytown, NY

Tiwald, T; Thompson, D; Woollam, J; Paulson, W & Hance, R. (1998). Application of IR variable angle spectroscopic ellipsometry to the determination of free carrier concentration depth profiles. *Thin Solid Films,* Vol. 313-314, No. pp. 661-666, ISSN 0040-6090

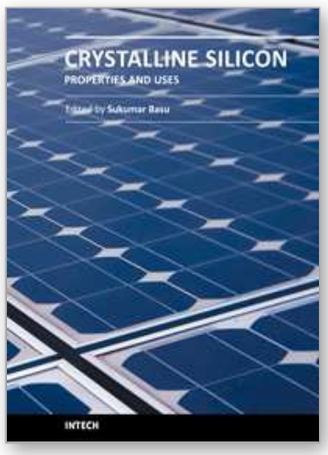

Crystalline Silicon - Properties and Uses
Edited by Prof. Sukumar Basu

ISBN 978-953-307-587-7
Hard cover, 344 pages
Publisher InTech
Published online 27, July, 2011
Published in print edition July, 2011

The exciting world of crystalline silicon is the source of the spectacular advancement of discrete electronic devices and solar cells. The exploitation of ever changing properties of crystalline silicon with dimensional transformation may indicate more innovative silicon based technologies in near future. For example, the discovery of nanocrystalline silicon has largely overcome the obstacles of using silicon as optoelectronic material. The further research and development is necessary to find out the treasures hidden within this material. The book presents different forms of silicon material, their preparation and properties. The modern techniques to study the surface and interface defect states, dislocations, and so on, in different crystalline forms have been highlighted in this book. This book presents basic and applied aspects of different crystalline forms of silicon in wide range of information from materials to devices.

InTech Europe
University Campus STeP Ri
Slavka Krautzeka 83/A
51000 Rijeka, Croatia
Phone: +385 (51) 770 447
Fax: +385 (51) 686 166
www.intechopen.com

InTech China
Unit 405, Office Block, Hotel Equatorial Shanghai
No.65, Yan An Road (West), Shanghai, 200040, China
中国上海市延安西路65号上海国际贵都大饭店办公楼405单元
Phone: +86-21-62489820
Fax: +86-21-62489821

IntechOpen